Surface & Coatings Technology 352 (2018) 370–377

Contents lists available at ScienceDirect

Surface & Coatings Technology

journal homepage: www.elsevier.com/locate/surfcoat

Study of the wettability behavior of stainless steel surfaces after ultrafast laser texturing

C. Sciancalepore[a,*], L. Gemini[b], L. Romoli[c], F. Bondioli[a,c]

[a] INSTM, Research Unit of Parma, Department of Industrial Engineering, University of Parma, Parco Area delle Scienze 181/A, 43124 Parma, Italy
[b] ALPhANOV, Institut d'Optique d'Aquitaine, Rue François Mitterrand, 33400 Talence, France
[c] Department of Engineering and Architecture, University of Parma, Parco Area delle Scienze 181/A, 43124 Parma, Italy

ARTICLE INFO

Keywords:
Superhydrophobicity
Laser
Biomimetic surface

ABSTRACT

The interest in superhydrophobic surfaces has grown exponentially over recent decades. Since the lotus leaf dual hierarchical structure was discovered, researchers have investigated the foundations of this behavior and many methods have been developed to obtain superhydrophobic surfaces. In this paper the possibility to use ultrafast laser treatments to obtain hydrophobic and superhydrophobic stainless surfaces was investigated on a AISI 316L stainless steel, ranging the total energy doses provided to the surfaces from 178 to 1143 J/cm^2. As SEM-FEG images reveals, different surface microstructures can be obtained at the increasing values of energy dose.

Independently on the specific values of laser treatment, all the obtained samples showed hydrophobic values of static contact angle. However, only particular surface microstructures allowed obtaining a self-cleaning surface characterized by low values of both contact angle hysteresis and roll-off angle.

The obtained results led to define the effect of the laser parameters on the morphological, chemical and wetting surface properties allowing one to design new textures with the desired wetting properties, from "lotus effect" surfaces to "rose petal effect" surfaces.

1. Introduction

The wettability of rough surfaces is a complex problem which continues to attract interest, thanks to new technologies and materials that allow obtaining surfaces with controlled micro- and nano-roughness [1]. Starting from the work of Neinhuis and Barthlott [2] that explained the origin of the superhydrophobicity and self-cleaning properties of the lotus leaf (the so-called "lotus effect"), a lot of efforts have been devoted to reproduce the micro and nano features of such surface, characterized by a water contact angle higher than 150° and, in general, low surface energy. Several techniques already exists to produce large-area superhydrophobic surfaces: transparent coatings have been developed for different kinds of window, as automobile windows [3], and eyeglasses, or to increase the performance of solar cells [4], to control bio-adhesion [5–7] and bio-fouling [8–10]. Nevertheless, most of these techniques, as for instance chemical vapor deposition (CVD) [11,12], electro-chemical deposition [13], and sol-gel method [14], involve the use of chemical coatings and show several drawbacks, especially in applications in which the release of coating particles into the environment is extremely critical. As an example, in food industry it is strategic that the coating used for tools undergoing chemical attack, scratches or wear, do not contaminate the products, which they contribute to cut, convey or package.

In this work, the possibility to use chemical-free ultrafast laser treatment to obtain hydrophobic and superhydrophobic stainless steel surfaces was investigated on AISI 316L, generally employed as food contact material. This technique offers several advantages over the other previously mentioned. Laser texturing is a one-step contactless approach that can be exploited with a flexible experimental apparatus, with the chance of creating a large variety of textures by tuning laser parameters and the environmental conditions [15,16].

This is the reason why, in the last five years, several approaches have been devoted to the fabrication of superhydrophobic surfaces using femtosecond lasers. Ultrashort laser pulses bring about an interaction process with the target material with a nearly negligible thermal transfer to the workpiece, allowing for a reproducible surface texture with virtually no heat affected zone [17]. Furthermore, such a technique can be potentially employed for the functionalization of large scale surfaces, with remarkable implications in the technological implementation. A thorough review of obtainable surface features as a function of the ruling process parameters can be found in [15,18]. Among the multiple functionalities that femtosecond lasers may induce

* Corresponding author.
E-mail address: corrado.sciancalepore@unimore.it (C. Sciancalepore).

https://doi.org/10.1016/j.surfcoat.2018.08.030
Received 13 April 2018; Received in revised form 16 July 2018; Accepted 9 August 2018
Available online 11 August 2018

within a surface, several contributions in literature exist showing the possibility to generate lotus-leaf like surfaces by ultrashort pulse laser texturing to modify the surface wettability [19]. One of the earliest and most comprehensive studies on the matter is due to Kietzig et al. [20] who realized ultrashort laser textures on AISI 304L stainless steel with static water contact angles (CA) between 120° and 150° and contact angle hysteresis (CAH) of 3°. A main finding of Kietzig et al. was that the superhydrophobic properties of the samples were discovered to be time-dependent. While the laser treated surfaces showed superhydrophilic behavior immediately after production for steel, titanium and aluminum, over the course of several weeks the wetting properties changed from superhydrophilic to superhydrophobic. Since surface roughness does not change with time, the reason of this behavior was attributed to surface chemical changes. In [20], the authors observed, by XPS analysis, that carbon and oxygen proportions of the surfaces changed in time, to which they attributed slow decomposition of carbon dioxide on the laser treated material surface. In a successive work [21], Kietzig et al. assert that the laser process causes a surface reaction, which changes the inherent wettability of pure metallic interfaces. The surface morphology after the treatment plays a minor role in the resulting contact angle as compared to surface chemistry changes.

Confirmation of the aforementioned findings was presented in [22], stating that the evolution of contact angles from superhydrophilic to superhydrophobic in the post laser treatment period was correlated with the amount of carbon on the structured surface and was independent of the chemical composition of the material. Nevertheless in [23], the explanation relating the increased superhydrophobicity to the amount of carbon on the surface was confirmed for aluminum substrates but not for steel. Conversely, the authors found that no hydrophobic functional groups were created on steel after laser treatment. Cunha et al. [24] found that laser treatment, carried out in air, led to the complete oxidation of both titanium and aluminum surfaces, which were reported to be hydrophilic. The equilibrium contact angles of these surfaces were similar or lower than 21°, the value reported by Kietzig et al. [20] for surfaces immersed in water after the laser treatment. Vorobyev and Guo [19] gave more importance to surface topography since laser-induced surface nanostructures play an important role in enhancing chemical interactions due to nanochemical effects, the first being oxidation of the ablated material and the second oxidation of the hot liquid/solid nanostructured surface after termination of ablation.

From the above state-of-the-art it is possible to see that despite experimental results showing that metal surfaces with tuned wettability are feasible by means of femtosecond lasers, the process is far from being completely understood.

A further complexity relates to the hypotheses of Vorobyev and Guo [19], who showed that lasers may create very different surface morphologies depending on the used parameters. Low laser fluence generates typical laser-induced periodic surface structures (LIPSS) on a submicron level. The apparent contact angle (CA) on surfaces covered by such features is generally lower than 150° [25]. With increasing laser fluence, periodic ripples and periodic cone-shaped spikes on a micron scale can be fabricated, both covered with LIPSS. The stainless steel surfaces with micro- and submicron double-scale structures have higher apparent Cas [26]. Rukosuyev et al. [27] found that by adjusting the fluences and with specific use of the focal volume of the laser beam, a micron scale ridge-like structure with superimposed submicron convex features could be produced. It was shown that the hydrophobic behavior was mainly caused by the surface texturing obtained as a result of laser ablation and not due to the intrinsic properties of the base materials.

From a topographic point of view, a multi-scale surface morphology made of nano- and micro-scale periodic ripples seems the best configuration to shift the wetting behavior to a superhydrophobic regime [28]. Nanoscale structures tend to become predominantly microscale with an increasing number of pulses and overlap [29]. While surface complexity increases, double-roughness patterns comprising nano- and micro-scale periodic ripples exhibited static CA > 150° and low CAH as well [30]. The high permanent superhydrophobicity of this pattern is due to the special micro/nano-structure of the surface that facilitates the Cassie–Baxter state, which led Fadeeva et al. [31] to create titanium lotus-like surface structures having self-cleaning properties than can even reduce the bacterial adhesion.

Based on this background, the aim of this work is to investigate the wetting properties of AISI 316L stainless steel surfaces textured by ultrashort pulse laser in order to establish the correlation between process parameters and physico-chemical behavior of the treated surfaces. A deeper understanding of the phenomena generated by the laser on metals is indeed fundamental for a reproducible process in view of industrial applications.

Moreover, it should be noted that texturing rates obtained to date do not allow treatment of large areas for practical industrial applications. As an example, the texturing rate of the pilot work of Kietzig et al. is about $7.5 \cdot 10^{-3}$ mm^2/s taking into account the scanning speed and laser spot diameter used in [20]. Such slow processing times would hinder any use of ultrafast laser technology over macro-scale mechanical components. Therefore, in view of increasing the overall process throughput, this work is focused on maximizing the scanning speed by making use of repetition rates up to 1 MHz, to guarantee sufficient pulse overlap to generate hierarchical nanofeatures at scanning speeds two orders of magnitude higher than those adopted so far.

The wetting behaviour, being dependent on both the surface roughness and the water–solid adhesion forces, were assessed by CA hysteresis, roll-off angle and surface energy measurements. In fact, it is now widely accepted that a superhydrophobic surface is adequately characterized when the advancing and receding CAs, which define the CAH, are measured together with the static CA in order to discriminate between the so-called “Lotus effect” (high CA and low CAH) and the “Rose petal effect” (high CA and high CAH). Finally, to define the effect of ageing on the surface properties, the wettability and the chemical properties were evaluated in time by static CA and X-ray photoelectron spectroscopy (XPS) measurements.

2. Experimental section

2.1. Femtosecond laser treatments

The irradiated samples consist of AISI 316L stainless steel square plates with lateral dimension of 50 mm and thickness of 2 mm. In order to disregard the influence of pre-existing surface roughness on the final results, the initial samples were mirror-polished with an as-received average roughness $S_a < 0.05$ μm. Before the laser treatment, the samples were washed for 5 min in acetone in an ultrasound bath, following which laser texturing was performed without shielding gas in line.

Textured areas with dimensions of 8 × 8 mm^2 were obtained with linearly horizontally polarized pulses from an Amplitude Systems Satsuma HP3 laser system. The system can deliver average power up to 40 W with repetition rate up to 1 MHz at central wavelength of 1030 nm and pulse duration of 320 fs. The emitted laser beam was firstly magnified by a factor of three through a beam expander and then directed into a scanning system to provide accurate positioning of the laser pulses, where it was finally focused on the sample surface by a 100 mm f-theta lens. The hatching strategy consisted of parallel lines on the sample surface, separated by the distance of 5 μm. Indicating with RR the laser repetition rate of the laser pulses and with v the scan speed, four different experimental conditions were examined: RR = 100 kHz and v = 200 mm/s (samples A), RR = 250 kHz and v = 500 mm/s (samples B), RR = 500 kHz and v = 1000 mm/s (samples C), and finally RR = 1000 kHz and v = 2000 mm/s (samples D). In this way the horizontal overlap d between successive pulses, given by $d = v/RR$, was kept constant at about 92%. For each value of repetition rate, the laser

Table 1
Experimental conditions and sample codes used for A sample (RR = 100 kHz).

Sample code	Repetition rate, RR (kHz)	Scan speed, v (mm/s)	Energy dose, E (J/cm^2) - 10 scans
A1	100	200	178
A2	100	200	235
A3	100	200	340
A4	100	200	423
A5	100	200	560
A6	100	200	663
A7	100	200	831
A8	100	200	950
A9	100	200	1143

fluence was varied from 0.36 to 2.33 J/cm^2. Defining energy dose, E, the ratio between the total energy provided to the surface by the radiation and the total irradiated area, the total energy dose provided in a single scan of the surfaces using the laser parameters specified above, ranged between 17,8 and 114,3 J/cm^2. Higher energy dose regimes can be achieved by superimposing multiple scans. In this work, the same process was repeated for 10 scans, therefore, by neglecting thermal losses between two consecutive passes, the total energy doses provided to the surfaces ranged from 178 to 1143 J/cm^2. In Table 1 the experimental conditions and the sample codes are summarized for the A samples. For all samples the letter identifies the RR and therefore the v, while the number following the letter, from 1 to 9, was used to identify the energy dose E for each set.

For the successive surface characterization, the treated surfaces were sonicated for 10 min in ethanol at room temperature, washed with fresh ethanol and finally dried in vacuum at room temperature.

2.2. Surface characterization

In order to evaluate the morphology of the nano-textured surfaces, scanning electron microscopy (SEM) characterizations were performed by a field emission SEM (FESEM, Nova NanoSEM 450, FEI company, USA). Low magnification (1500–6000 ×) images were acquired in field-free lens mode using the Everhart-Thornley detector (ETD) (conventional "below-the-lens" detector) for the secondary electron (SE) imaging signal. High magnification (10,000–400,000 ×) images were obtained in immersion lens mode using the "through-the-lens" detector (TLD) for the down-hole visibility (DHV) imaging mode. The accelerating voltage (HV) of 20 kV, the spot size of 3 and the working distance (WD) of 6 mm were used in the acquisition of all images.

Chemical elemental analysis was performed with the energy-dispersive X-ray spectroscopy system (X-EDS) QUANTAX-200 (Bruker, Germany), equipped with the silicon drift detector (SDD) XFlash 6/10.

To evaluate the wettability behavior of the surfaces the full characterization of wetting properties, including static and dynamic contact angles (CA), roll-off angle and surface free energy, were performed using the contact angle meter OCA 20 (DataPhysics Instruments Gmbh, Filderstadt, Germany) under room condition.

Static water CAs were determined by sessile drop method on the basis of at least 3 measurements with a drop volume of 1 μl using distilled deionized water. The behavior of the CA values was monitored periodically for 120 days after the laser treatment. The new measurements were made using always fresh surface, storing the samples at room conditions without any further cleaning treatment that could modify the surface properties.

In the dynamic CA analysis, the advancing/receding CAs were measured using the sessile drop (needle in) method by adding/removing liquid (8 μl) to/from the initially deposited droplet (starting volume 4 μl) at a very small volume flow rate (0.1 μl/s), in order to obtaining the quasi-static equilibrium condition during the phase of expansion and contraction of the droplet volume. Contact angle hysteresis was determined by comparing the advancing and receding CAs of the growing and shrinking droplet.

In the roll-off measurements, a 10 μl drop was initially deposited on the surface, which was subsequently inclined at a constant speed of 0.3°/sec, until the drop was completely slipped away. The dynamic process of the drop shedding off surface was followed by a high-speed CCD camera.

The surface energy was evaluated by the method of Owen et al. [32], according to which the interfacial tension derives from the underlying interactions between the molecules. The surface energy of the textured surface is obtained by benchmarking with the CA values of the same surface obtained with specific fluids with well-known surface energy values (in this study water, formamide and diiodomethane).

Finally, to evaluate the evolution in time of the surface elemental composition, XPS measurements were carried with a XR3 dual anode X-ray source of Vacuum Generators, delivering Mg Kα photons (energy = 1253.6 eV), operated at 15 kV, 18 mA. Spectra were acquired with a Perkin Elmer, model 15-255-G, double pass cylindrical mirror analyzer (CMA) driven at constant pass energy of 100 eV (2 eV resolution) for wide spectra and at 50 eV of pass energy (1 eV resolution) for elemental spectra. Ageing effects on treated samples were checked by taking the same sequence of XPS spectra, after 1, 3, 10 and 30 days in air. To avoid perturbation of surface composition, no sputtering-cleaning to remove contaminants form air exposure was applied to the samples before analysis.

3. Result and discussion

3.1. Evolution of surface wettability with laser-induced surface morphology

In Fig. 1 SEM-FEG images of surfaces obtained with different values of RR and for increasing values of energy doses, E, are reported. At low energy doses, periodic surfaces structures, also known as LIPSS (Laser Induced Periodic Surface Structures) [33], which are oriented perpendicularly to the laser polarization and with a period comparable to the laser wavelength, are visible. The presence of LIPSS on steel in similar conditions of irradiation was previously assessed [34]. By increasing the energy dose E, LIPSS leave place to columnar structures whose transversal dimension, increase independently on RR. For example, for A samples (RR = 100 kHz), the transversal dimension ranges from 5 ± 2 μm when E is 423 J/cm^2 to 10 ± 2 μm when E is 1143 J/cm^2.

Interestingly, the same morphological evolution, that is an increase of the transversal dimension of the columnar structures, is observed for increasing RR at constant E values. For example, for a dose of 1143 J/cm^2, the transversal dimension ranges from 10 ± 2 μm in samples A (RR = 100 kHz) to 24 ± 4 μm in samples D (RR = 1000 kHz). This behaviour could be due to thermal effects related to an increase of both RR or E [15].

A further increase of the magnification allowed one to observe features with nanometric dimensions overimposed on the surface of LIPSS. In Fig. 2 SEM-FEG images of C samples (RR = 500 kHz) as a function of dose are reported at different magnifications. The higher magnification allowed one to underline that the microstructure are covered by finer structures mainly constituted by spherical shaped particles whose size is in the nanometer scale [33].

In Table 2 the static water CA values 30 days after the laser treatment as a function of dose for the four different experimental conditions A–D, are reported. The results underline that the laser treatment increases the water CA of the surface from 77 ± 3°, characteristic of the untreated 316L steel, to values well above 140°. Independently on the specific values of RR, v and dose, it is possible to reach hydrophobic values of CA: in the studied conditions, the stabilized CA do not show a strong connection and dependency on the specific microstructure [10] but, in agreement with [26], could be associated to the characteristic double-scale microstructure.

In order to better understand the relationship between the

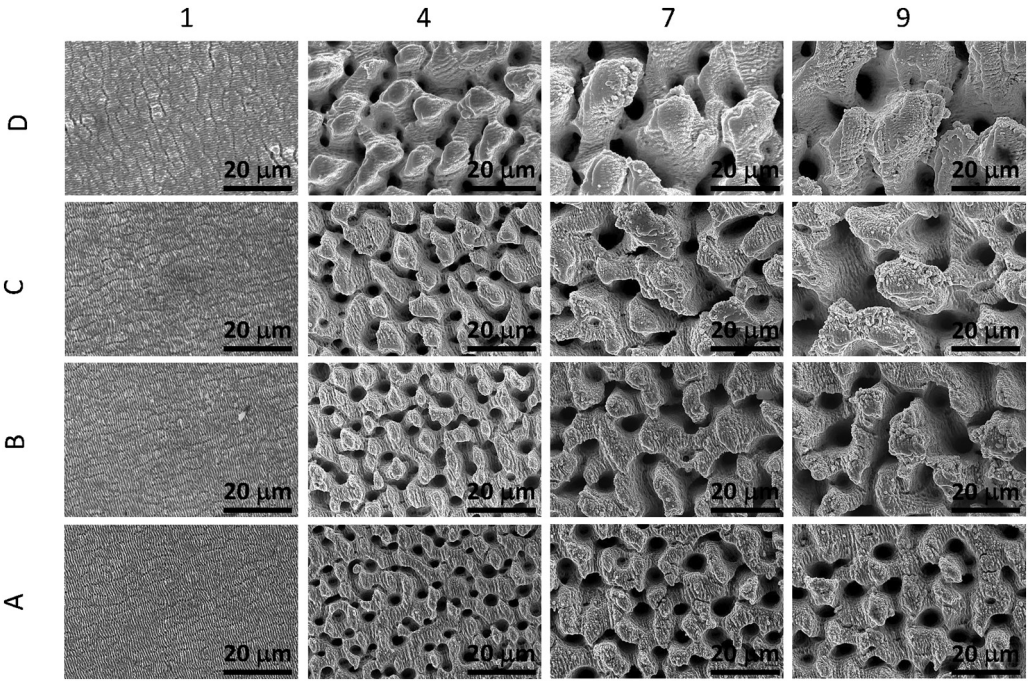

Fig. 1. SEM-FEG images of the treated samples as a function of dose, E (1 = 178 J/cm^2; 4 = 423 J/cm^2; 7 = 831 J/cm^2; 9 = 1143 J/cm^2), and repetition rate, RR (A = 100 kHz; B = 250 kHz; C = 500 kHz; D = 1000 kHz).

hierarchical surface structures and the surface wettability, four samples of the C set (RR 500 kH), were further characterized: sample C1, C4, C7 and C9 were chosen for the measurements of dynamic CA values, roll-angle and surface energy (Table 3).

Sample C1, obtained with the lower energy dose, is characterized by the highest hysteresis and surface energy and absence of roll-off angle. The LIPSS structure visible on the sample surface (Fig. 1, sample C1) leads to high surface energy value, due to both dispersive (van der Waals and other non-site-specific intermolecular forces) and polar (dipole–dipole, dipole-induced dipole, hydrogen bonding and other site-specific forces) interactions [35], allowing to obtain a "rose petal effect" surface, as demonstrated by the roll off angle measurement. In this case, the water drop shows high CA but remains anchored to the surface even when the sample is tilted of 180°. As the energy dose increases, the microstructure becomes columnar and bumps appear: the interaction

Table 2
Water CA values as a function of dose for the four different experimental conditions, measured 30 days after the laser treatment (A: RR 100 kHz; B: RR 250 kHz; C: RR 500 kHz; D: RR 1000 kHz).

Water contact angle values (°)					
Dose (J/cm^2)	Codes	Set A	Set B	Set C	Set D
178,0	1	151 ± 5	149 ± 5	149 ± 5	143 ± 5
234,6	2	145 ± 5	157 ± 5	165 ± 5	152 ± 5
339,8	3	165 ± 5	165 ± 5	162 ± 5	160 ± 5
423,0	4	164 ± 5	163 ± 5	164 ± 5	157 ± 5
560,0	5	160 ± 5	160 ± 5	160 ± 5	158 ± 5
663,0	6	163 ± 5	155 ± 5	161 ± 5	158 ± 5
831,0	7	160 ± 5	161 ± 5	161 ± 5	156 ± 5
950,0	8	152 ± 5	150 ± 5	163 ± 5	156 ± 5
1143,0	9	160 ± 5	162 ± 5	160 ± 5	155 ± 5

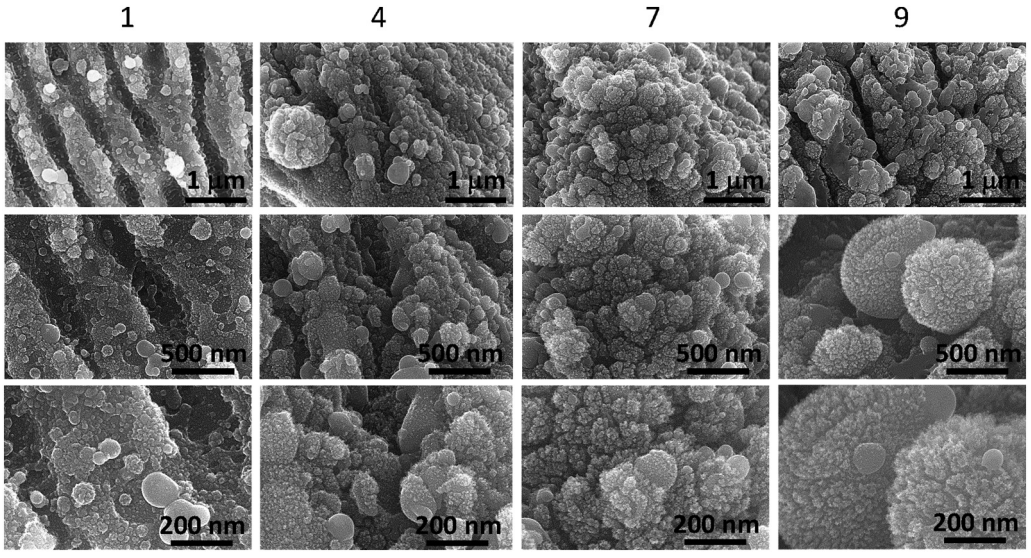

Fig. 2. SEM-FEG images of C samples (RR = 500 kHz) as function of the dose at different magnifications.

Table 3
Dynamic water CA values, hysteresis, roll off angle and surface energy values of sample C1 (E 178 J/cm^2), C4 (E 423 J/cm^2), C7 (E 831 J/cm^2) and C9 (E 1143 J/cm^2) obtained at RR 500 kHz, one month after the laser treatment.

Sample codes	Surface morphology	Advancing CA (°)	Receding CA (°)	Hysteresis (°)	Roll-off angle (°)	Surface energy [m/Nm]
C1	LIPSS	159(2)	130(1)	29(2)	No roll off	41.9
C4	Fine bumps	164(2)	149(3)	14(2)	11(1)	17.4
C7	Medium bumps	164(3)	145(3)	20(2)	16(3)	38
C9	Large bumps	164(1)	145(1)	19(2)	20(2)	39.8

liquid-surface changes importantly. The sample C4, characterized by a fine columnar structure (Fig. 1, sample C4), shows the lowest values of hysteresis and surface energy with a roll off angle of 11°, characteristic values for a self-cleaning surface. In this case, the water drop quickly rolls off the surface even for negligible tilting of the sample. As the dose further increase, together with the average size of the bumps (Fig. 1, sample C7 and C9), also the liquid/solid contact area increases, and the surface presents higher surface energy, comparable with those exhibited by LIPSS, a pronounced hysteresis and roll-off angle higher than 15°.

3.2. Evolution of surface wettability with laser-induced surface chemistry

It has been already reported by Kietzig et al. [20] that after femtosecond laser irradiation, AISI 304L shows initially a superhydrophilic state that becomes superhydrophobic in time several days after the laser process. In this work, to confirm this behavior on AISI 316L samples, treated with the previously introduced process parameters, water CA measurements were carried each 7 days for 120 days after the laser treatment. Fig. 3 presents the behavior of water CA as a function of time for the four samples (C1, C4, C7 and C9) previously mentioned.

Ten days after the laser texturing process, all samples reach a hydrophobic state regardless the specific process parameters, or surface morphology. The visible difference between the wetting behavior of the different cases is observed a few days after the laser texturing process (Day 3) only, where the surface shows a more hydrophilic behavior as the energy dose increases from sample C1 to sample C9. These results are in good agreement with [20], where the time needed for the samples to reach the steady state increases with increasing fluence.

This behavior is explained by an evolution in time of the surface chemistry, initiate by the ultra-fast interaction with the laser pulses and due to the exposition to air environment [20]. To evaluate the chemistry behavior of the surfaces, XPS measurement were performed on the selected samples immediately after the laser treatment as well as 1, 3, 10 and 30 days later. Fig. 4 presents the XPS spectra of the laser treated samples, where iron, oxygen and carbon peaks are clearly visible.

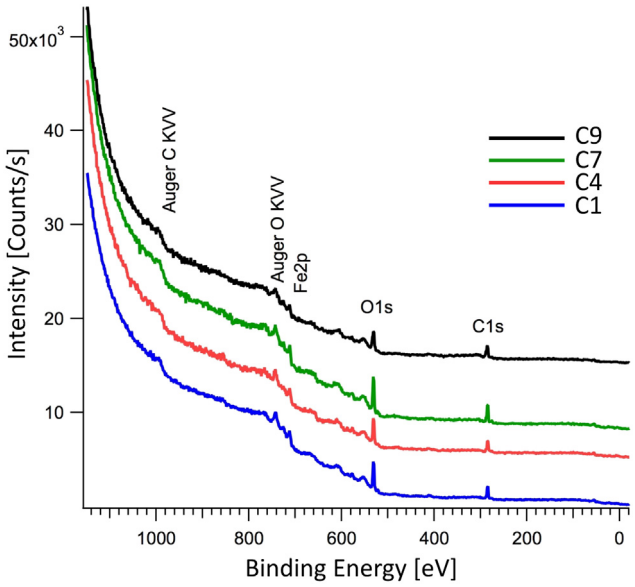

Fig. 4. XPS spectra of the as treated samples (RR 500 kHz; C1 178 J/cm^2; C4 423 J/cm^2; C7 831 J/cm^2; C9 1143 J/cm^2).

The spectra of the different elements (Fig. 5, sample C9 as representative) do not present any sizeable difference in line shape

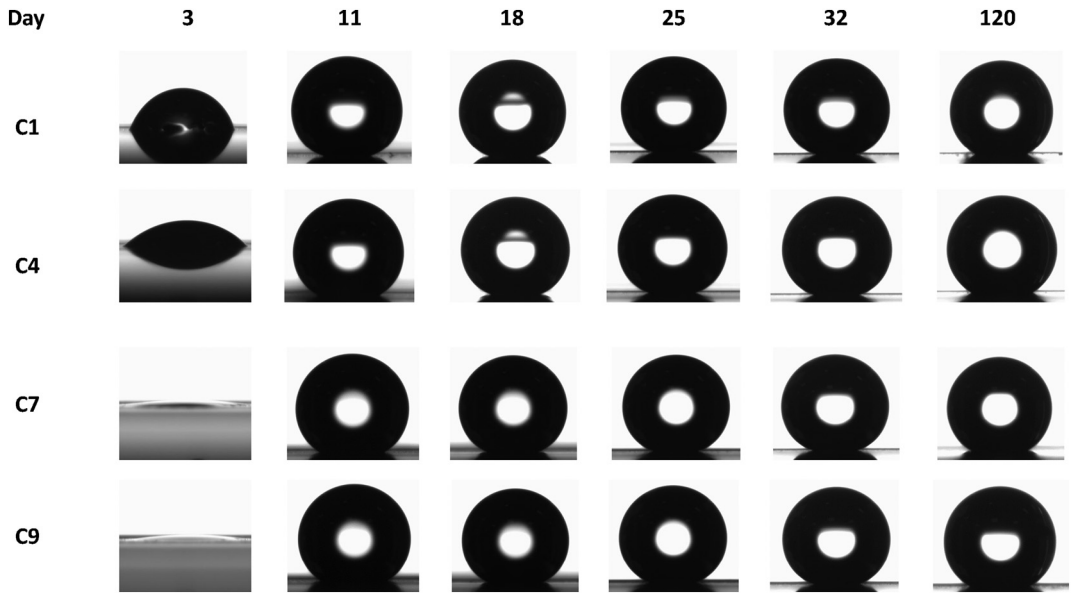

Fig. 3. Water CA behavior as a function of time for samples treated a RR 500 kHz (C1 178 J/cm^2; C4 423 J/cm^2; C7 831 J/cm^2; C9 1143 J/cm^2).

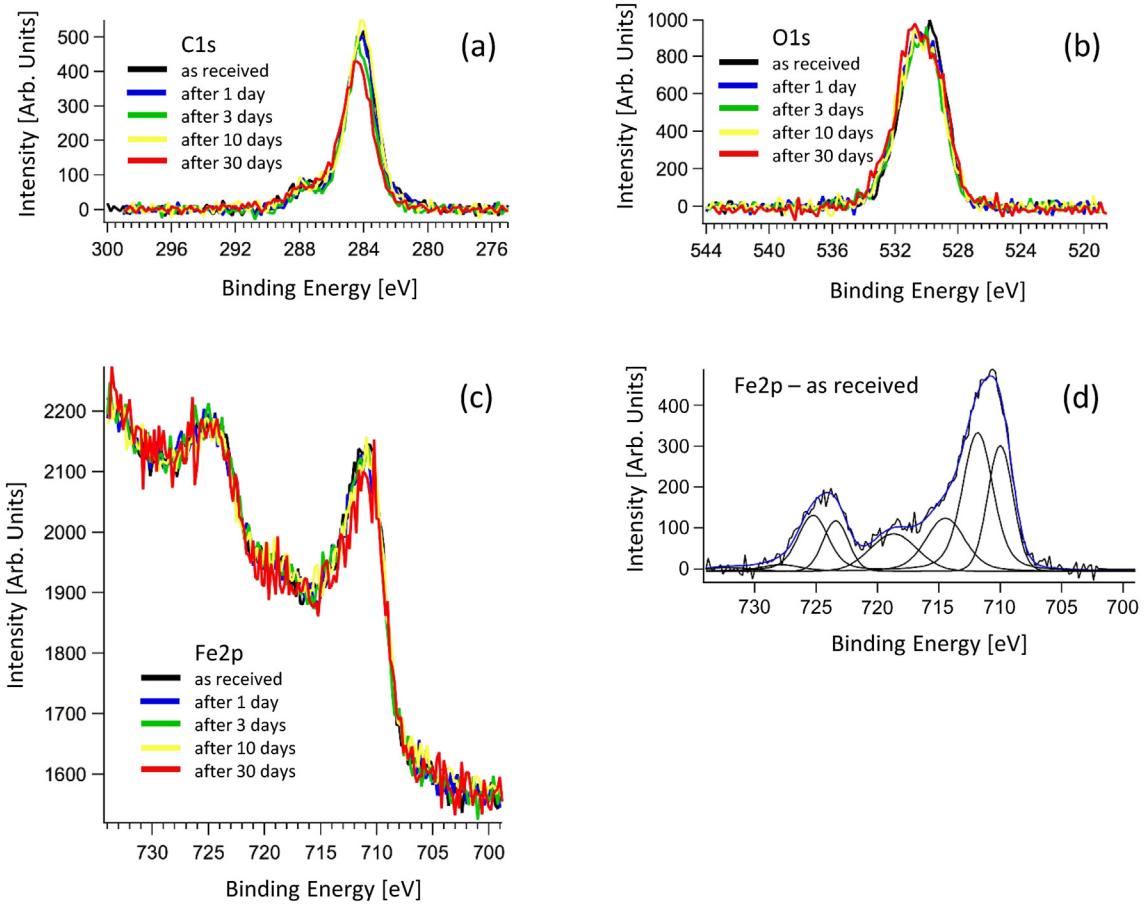

Fig. 5. XPS spectra in the regions of C1s (a), O1s (b), and Fe2p (c) of sample C9 as a function of ageing time in air. For the 'as received' spectrum of Fe2p (d), the background subtracted Fe2p features are also reported, together with their fit-decomposition into Voigt peaks.

following ageing in air. In general, C1s spectra present a main structure centered at about 284.3 eV that can be associated to C—C and C—H bonds. Oxidized C (C—O and C═O bonds) is represented by the high binding energy shoulder of the main structure. This do not appear to vary between different morphologies nor following ageing in air. O1s spectra present a broad peak that can be associated to oxidized carbon species, but also to OH and to possible H_2O contribution. Finally, Fe2p multiple is relatively broad. The line shape can be associated to a prevalence of Fe (III), but with contributions of Fe (II). Analogous results were obtained for all the other spectra here not reported.

By following the intensity of the XPS peaks, the relative concentration of the elemental species at the surface can be determined taking into account the appropriate atomic sensitivity factors for the used analyzer. Results are reported in Table 4.

As a general trend it can be observed that 30 days after the laser process, the amount of oxygen tends to decrease, while the amount of carbon increases. Only a small decrease of the Fe peak is observed (here not reported). The carbon and oxygen contents measured on the same day, do not significantly change between different samples, that is they are independent from the dose and, therefore from the specific morphology.

Table 4
Oxygen and carbon content of sample C1 (E 178 J/cm^2), C4 (E 423 J/cm^2), C7 (E 831 J/cm^2) and C9 (E 1143 J/cm^2) obtained by XPS curve analysis.

Days samples	Oxygen content (%)				Carbon content (%)			
	C1	C4	C7	C9	C1	C4	C7	C9
0	38	39	37	38	54	54	54	53
1	38	32	33	35	54	61	60	57
3	34	38	37	37	59	55	56	54
10	36	38	37	37	57	55	56	56
30	31	30	30	28	64	64	65	67

Fig. 6b and c present a comparison between the evolution in time of the static CA and the C and O contents, respectively. SEM images of the surface morphologies are reported in Fig. 6a for easier comparison. The connection between the evolution of the CA with the chemical state of the surface is quite straightforward. About ten days after the laser texturing process, the CA values begin to stabilize followed by an increase of C content which starts to take place on the steel surface. As the elemental composition of the surface keeps evolving, the surface state finally reaches a stable hydrophobic behavior after about 30 days, as already observed in Fig. 3, regardless the its specific morphology. This result demonstrates that the key parameter driving the steel surface state to a hydrophobic one is the evolution of the chemical state which takes place on the stainless steel surface as a consequence of the interaction with the laser light.

The role of the specific surface morphology is to discriminate the roll-off behavior of the surface. As previously observed in Table 3, although LIPSS and bumps morphologies are both characterized by high CA values, the main difference lies in the roll-off angle values. LIPSS show no-roll off, that is the liquid drop do not spread on the surface but do not move easily from the contact point; on the other hand, when the liquid drop is placed on a fine bumpy surface, it roll-off quickly from the contact point, making the surface self-cleaning.

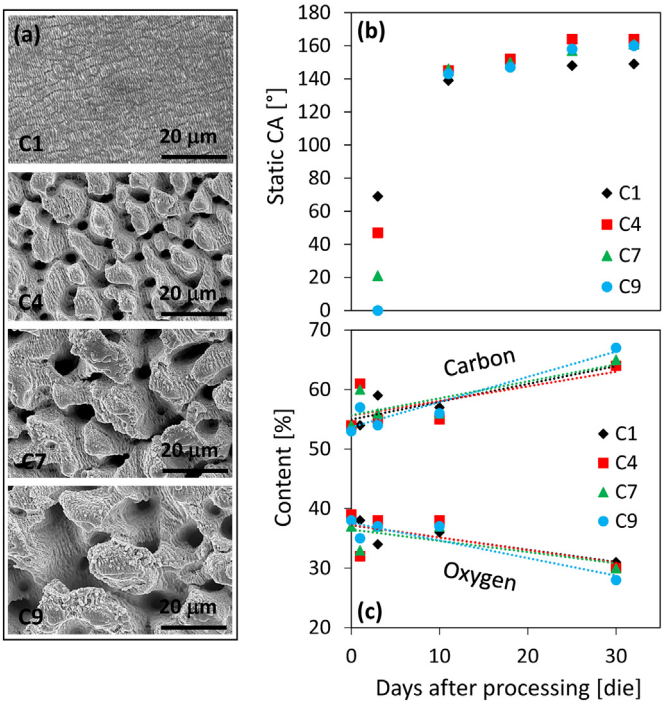

Fig. 6. Comparison among the surface morphology (a) and the evolution of both static CA (b) and C and O content (c) with the time for the C1–C9 samples.

4. Conclusion

The obtained results demonstrated that all the experimental conditions allowed to obtain AISI 316L stainless steel surfaces with very high static CA, about 30 days after laser treatment. Different nano and microstructures can be obtained by changing the laser parameters (RR, v and dose), leading to surfaces characterized by high CA and low hysteresis (lotus effect) or by high CA and high hysteresis (rose-petal effect) demonstrating the key role of laser parameter to obtain self-cleaning surfaces. In this sense, a structure characterized by fine bumps (transverse dimension of about 10 µm) allows to obtain a super-hydrophobic surface where water droplets roll-off quickly from the contact point. In particular, sample C4, obtained with an energy dose of 423 J/cm^2, can be considered the best self-cleaning sample having surface properties similar to those of a lotus leaf.

Regarding the wettability behavior with time, results demonstrate the effect of the surface chemistry: the laser-material interaction activates the surface in a way that its oxygen content after the laser treatment is high leading to an hydrophilic state that however evolves to hydrophobic, regardless the specific surface morphology, in 10 days after the laser texturing process.

Finally, this work shows once again that femtosecond laser machining might be a large-scale alternative to chemical approaches to obtain superhydrophobic textures on stainless steel.

Acknowledgements

This project has received funding from the European Union's Horizon 2020 Research and Innovation Programme under Grant Agreement No 687613.

References

[1] E. Celia, T. Darmanin, E. Taffin de Givenchy, S. Amigoni, F. Guittard, Recent advances in designing superhydrophobic surfaces, J. Colloid Interface Sci. 402 (2013) 1–18, https://doi.org/10.1016/j.jcis.2013.03.041.
[2] C. Neinhuis, W. Barthlott, Characterization and distribution of water-repellent, self-cleaning plant surfaces, Ann. Bot. 79 (1997) 667–677, https://doi.org/10.1006/anbo.1997.0400.
[3] Y. Xu, W.H. Fan, Z.H. Li, D. Wu, Y.H. Sun, Antireflective silica thin films with super water repellence via a solgel process, Appl. Opt. 42 (2003) 108–112, https://doi.org/10.1364/AO.42.000108.
[4] G.R.J. Artus, S. Jung, J. Zimmermann, H.P. Gautschi, K. Marquardt, S. Seeger, Silicone nanofilaments and their application as superhydrophobic coatings, Adv. Mater. 18 (2006) 2758–2762, https://doi.org/10.1002/adma.200502030.
[5] P. Roach, N.J. Shirtcliffe, D. Farrar, C.C. Perry, Quantification of surface-bound proteins by fluorometric assay: comparison with quartz crystal microbalance and amido black assay, J. Phys. Chem. B 110 (2006) 20572–20579, https://doi.org/10.1021/jp0621575.
[6] J. Heitz, C. Plamadeala, M. Muck, O. Armbruster, W. Baumgartner, A. Weth, C. Steinwender, H. Blessberger, J. Kellermair, S.V. Kirner, J. Krüger, J. Bonse, A.S. Guntner, A.W. Hassel, Femtosecond laser-induced microstructures on Ti substrates for reduced cell adhesion, Appl. Phys. A Mater. Sci. Process. 123 (2017), https://doi.org/10.1007/s00339-017-1352-0.
[7] S.V. Kirner, U. Hermens, A. Mimidis, E. Skoulas, C. Florian, F. Hischen, C. Plamadeala, W. Baumgartner, K. Winands, H. Mescheder, J. Krüger, J. Solis, J. Siegel, E. Stratakis, J. Bonse, Mimicking bug-like surface structures and their fluid transport produced by ultrashort laser pulse irradiation of steel, Appl. Phys. A Mater. Sci. Process. 123 (2017), https://doi.org/10.1007/s00339-017-1317-3.
[8] H. Zhang, R. Lamb, J. Lewis, Engineering nanoscale roughness on hydrophobic surface - preliminary assessment of fouling behaviour, Sci. Technol. Adv. Mater. (2005) 236–239, https://doi.org/10.1016/j.stam.2005.03.003.
[9] A. Elbourne, R.J. Crawford, E.P. Ivanova, Nano-structured antimicrobial surfaces: from nature to synthetic analogues, J. Colloid Interface Sci. 508 (2017) 603–616, https://doi.org/10.1016/j.jcis.2017.07.021.
[10] F.H. Rajab, C.M. Liauw, P.S. Benson, L. Li, K.A. Whitehead, Picosecond laser treatment production of hierarchical structured stainless steel to reduce bacterial fouling, Food Bioprod. Process. 109 (2018) 29–40, https://doi.org/10.1016/j.fbp.2018.02.009.
[11] K.K.S. Lau, J. Bico, K.B.K. Teo, M. Chhowalla, G.A.J. Amaratunga, W.I. Milne, G.H. McKinley, K.K. Gleason, Superhydrophobic carbon nanotube forests, Nano Lett. 3 (2003) 1701–1705, https://doi.org/10.1021/nl034704t.
[12] H. Tavana, A. Amirfazli, A.W. Neumann, Fabrication of superhydrophobic surfaces of n-hexatriacontane, Langmuir 22 (2006) 5556–5559, https://doi.org/10.1021/la0607757.
[13] X. Zhang, F. Shi, J. Niu, Y. Jiang, Z. Wang, Superhydrophobic surfaces: from structural control to functional application, J. Mater. Chem. 18 (2008) 621–633, https://doi.org/10.1039/B711226B.
[14] R. Taurino, E. Fabbri, M. Messori, F. Pilati, D. Pospiech, A. Synytska, Facile preparation of superhydrophobic coatings by sol-gel processes, J. Colloid Interface Sci. 325 (2008) 149–156, https://doi.org/10.1016/j.jcis.2008.05.007.
[15] F. Fraggelakis, G. Mincuzzi, J. Lopez, I. Manek-Hönninger, R. Kling, Texturing metal surface with MHz ultra-short laser pulses, Opt. Express 25 (2017) 18131, https://doi.org/10.1364/OE.25.018131.
[16] E. Skoulas, A. Manousaki, C. Fotakis, E. Stratakis, Biomimetic surface structuring using cylindrical vector femtosecond laser beams, Sci. Rep. 7 (2017), https://doi.org/10.1038/srep45114.
[17] E. Toyserkani, N. Rasti, Ultrashort pulsed laser surface texturing, Laser Surf. Eng. Process. Appl. (2014) 441–453, https://doi.org/10.1016/B978-1-78242-074-3.00018-0.
[18] K.M. Tanvir Ahmmed, C. Grambow, A.M. Kietzig, Fabrication of micro/nano structures on metals by femtosecond laser micromachining, Micromachines. 5 (2014) 1219–1253, https://doi.org/10.3390/mi5041219.
[19] A.Y. Vorobyev, C. Guo, Multifunctional surfaces produced by femtosecond laser pulses multifunctional surfaces produced by femtosecond laser pulses, J. Appl. Phys. 33103 (2015), https://doi.org/10.1063/1.4905616.
[20] A.M. Kietzig, S.G. Hatzikiriakos, P. Englezos, Patterned superhydrophobic metallic surfaces, Langmuir 25 (2009) 4821–4827, https://doi.org/10.1021/la8037582.
[21] A.M. Kietzig, M.N. Mirvakili, S. Kamal, P. Englezos, S.G. Hatzikiriakos, Laser-patterned super-hydrophobic pure metallic substrates: Cassie to Wenzel wetting transitions, J. Adhes. Sci. Technol. 25 (2012) 2789–2809, https://doi.org/10.1163/016942410X549988.
[22] H. Kenar, E. Akman, E. Kacar, A. Demir, H. Park, H. Abdul-Khaliq, C. Aktas, E. Karaoz, Femtosecond laser treatment of 316L improves its surface nanoroughness and carbon content and promotes osseointegration: an in vitro evaluation, Colloids Surf. B: Biointerfaces 108 (2013) 305–312, https://doi.org/10.1016/j.colsurfb.2013.02.039.
[23] P. Bizi-Bandoki, S. Valette, E. Audouard, S. Benayoun, Time dependency of the hydrophilicity and hydrophobicity of metallic alloys subjected to femtosecond laser irradiations, Appl. Surf. Sci. 273 (2013) 399–407, https://doi.org/10.1016/j.apsusc.2013.02.054.
[24] A. Cunha, A.P. Serro, V. Oliveira, A. Almeida, R. Vilar, M.C. Durrieu, Wetting behaviour of femtosecond laser textured Ti-6Al-4V surfaces, Appl. Surf. Sci. 265 (2013) 688–696, https://doi.org/10.1016/j.apsusc.2012.11.085.
[25] B. Wu, M. Zhou, J. Li, X. Ye, G. Li, L. Cai, Superhydrophobic surfaces fabricated by microstructuring of stainless steel using a femtosecond laser, Appl. Surf. Sci. 256 (2009) 61–66, https://doi.org/10.1016/j.apsusc.2009.07.061.
[26] S. Sarbada, Y.C. Shin, Superhydrophobic contoured surfaces created on metal and polymer using a femtosecond laser, Appl. Surf. Sci. 405 (2017) 465–475, https://doi.org/10.1016/j.apsusc.2017.02.019.
[27] M.V. Rukosuyev, J. Lee, S.J. Cho, G. Lim, M.B.G. Jun, One-step fabrication of superhydrophobic hierarchical structures by femtosecond laser ablation, Appl. Surf. Sci. 313 (2014) 411–417, https://doi.org/10.1016/j.apsusc.2014.05.224.
[28] P. Bizi-Bandoki, S. Benayoun, S. Valette, B. Beaugiraud, E. Audouard, Modifications

of roughness and wettability properties of metals induced by femtosecond laser treatment, Appl. Surf. Sci. (2011) 5213–5218, https://doi.org/10.1016/j.apsusc.2010.12.089.
[29] R. Jagdheesh, B. Pathiraj, E. Karatay, G.R.B.E. Römer, A.J. Huis In'T Veld, Laser-induced nanoscale superhydrophobic structures on metal surfaces, Langmuir 27 (2011) 8464–8469, https://doi.org/10.1021/la2011088.
[30] S. Moradi, S. Kamal, P. Englezos, S.G. Hatzikiriakos, Femtosecond laser irradiation of metallic surfaces: effects of laser parameters on superhydrophobicity, Nanotechnology 24 (2013), https://doi.org/10.1088/0957-4484/24/41/415302.
[31] E. Fadeeva, V.K. Truong, M. Stiesch, B.N. Chichkov, R.J. Crawford, J. Wang, E.P. Ivanova, Bacterial retention on superhydrophobic titanium surfaces fabricated by femtosecond laser ablation, Langmuir 27 (2011) 3012–3019, https://doi.org/10.1021/la104607g.
[32] D.K. Owens, R.C. Wendt, Estimation of the surface free energy of polymers, J. Appl. Polym. Sci. 13 (1969) 1741–1747, https://doi.org/10.1002/app.1969.070130815.
[33] J. Bonse, J. Krüger, S. Höhm, A. Rosenfeld, Femtosecond laser-induced periodic surface structures, J. Laser Appl. 24 (2012) 42006, https://doi.org/10.2351/1.4712658.
[34] G. Mincuzzi, L. Gemini, M. Faucon, R. Kling, Extending ultra-short pulse laser texturing over large area, Appl. Surf. Sci. 386 (2016) 65–71, https://doi.org/10.1016/j.apsusc.2016.05.172.
[35] R.J. Good, Contact angle, wetting, and adhesion: a critical review, J. Adhes. Sci. Technol. 6 (1992) 1269–1302, https://doi.org/10.1163/156856192X00629.